



Co-culture cell-derived extracellular matrix loaded electrospun microfibrillar scaffolds for bone tissue engineering

Marta S. Carvalho^{a,b,d,1}, João C. Silva^{a,c,d,1}, Ranodhi N. Udangawa^c, Joaquim M.S. Cabral^{a,d}, Frederico Castelo Ferreira^{a,d}, Cláudia L. da Silva^{a,d}, Robert J. Linhardt^{b,c,*}, Deepak Vashishth^{b,**}

^a Department of Bioengineering and iBB - Institute of Bioengineering and Biosciences, Instituto Superior Técnico, Universidade de Lisboa, Av. Rovisco Pais, Lisboa 1049-001, Portugal

^b Department of Biomedical Engineering, Center for Biotechnology and Interdisciplinary Studies, Rensselaer Polytechnic Institute, Troy, NY 12180-3590, USA

^c Department of Chemistry and Chemical Biology, Biological Sciences and Chemical and Biological Engineering, Center for Biotechnology and Interdisciplinary Studies, Rensselaer Polytechnic Institute, Troy, NY 12180-3590, USA

^d The Discoveries Centre for Regenerative and Precision Medicine, Lisbon Campus, Instituto Superior Técnico, Universidade de Lisboa, Av. Rovisco Pais, Lisboa 1049-001, Portugal

ARTICLE INFO

Keywords:

Cell-derived extracellular matrix
Electrospinning
Mesenchymal stem/stromal cells
Human umbilical vein endothelial cells
Bone tissue engineering

ABSTRACT

Cell-derived extracellular matrix (ECM) has been employed as scaffolds for tissue engineering, creating a bio-mimetic microenvironment that provides physical, chemical and mechanical cues for cells and supports cell adhesion, proliferation, migration and differentiation by mimicking their *in vivo* microenvironment. Despite the enhanced bioactivity of cell-derived ECM, its application as a scaffold to regenerate hard tissues such as bone is still hampered by its insufficient mechanical properties. The combination of cell-derived ECM with synthetic biomaterials might result in an effective strategy to enhance scaffold mechanical properties and structural support. Electrospinning has been used in bone tissue engineering to fabricate fibrous and porous scaffolds, mimicking the hierarchical organized fibrillar structure and architecture found in the ECM. Although the structure of the scaffold might be similar to ECM architecture, most of these electrospun scaffolds have failed to achieve functionality due to a lack of bioactivity and osteoinductive factors. In this study, we developed bioactive cell-derived ECM electrospun polycaprolactone (PCL) scaffolds produced from ECM derived from human mesenchymal stem/stromal cells (MSC), human umbilical vein endothelial cells (HUVEC) and their combination based on the hypothesis that the cell-derived ECM incorporated into the PCL fibers would enhance the biofunctionality of the scaffold. The aims of this study were to fabricate and characterize cell-derived ECM electrospun PCL scaffolds and assess their ability to enhance osteogenic differentiation of MSCs, envisaging bone tissue engineering applications. Our findings demonstrate that all cell-derived ECM electrospun scaffolds promoted significant cell proliferation compared to PCL alone, while presenting similar physical/mechanical properties. Additionally, MSC:HUVEC-ECM electrospun scaffolds significantly enhanced osteogenic differentiation of MSCs as verified by increased ALP activity and osteogenic gene expression levels. To our knowledge, these results describe the first study suggesting that MSC:HUVEC-ECM might be developed as a biomimetic electrospun scaffold for bone tissue engineering applications.

1. Introduction

The extracellular matrix (ECM) is composed of a complex and highly organized assembly of biomolecules, such as fibrillary proteins (e.g. collagens, fibronectin, laminin), glycosaminoglycans (e.g. heparan

sulfate, chondroitin sulfate, hyaluronan), proteoglycans (e.g. decorin, versican, aggrecan) and matricellular proteins (e.g. osteopontin, thrombospondin) [1,2]. Although being composed mainly by the above-mentioned components, ECM composition and distribution of the matrix molecules vary considerably with the type of tissue and can be

* Correspondence to: R.J. Linhardt, Department of Biomedical Engineering, Center for Biotechnology and Interdisciplinary Studies, Rensselaer Polytechnic Institute, Troy, NY 12180-3590, USA.

** Corresponding author.

E-mail addresses: linhar@rpi.edu (R.J. Linhardt), vashid@rpi.edu (D. Vashishth).

¹ These authors contributed equally to the work.

<https://doi.org/10.1016/j.msec.2019.01.127>

Received 22 September 2018; Received in revised form 25 January 2019; Accepted 28 January 2019

Available online 30 January 2019

0928-4931/ © 2019 Elsevier B.V. All rights reserved.

altered during the stages of tissue development and due to pathological conditions [1].

Currently, tissue engineering and regenerative medicine is focused on developing biomaterials that can mimic the native ECM by incorporating features that recapitulate its architecture, structure, composition and functionality, recreating the *in vivo* microenvironment. In fact, some isolated ECM components, such as collagen, fibronectin, vitronectin, and glycosaminoglycans [3–7], have been used in the design of new biomaterial scaffolds. However, these proteins alone fail to achieve the molecular complexity of the native ECM. Moreover, most of the secreted factors and ECM molecules are still unknown or have an unknown biological concentration, thus, hindering the development of optimized cell culture media. Therefore, using the whole cell-derived ECM appears a promising alternative approach to better mimic the *in vivo* microenvironment of tissues [8,9]. Additionally, cell-derived ECM serves as a reservoir of multiple cytokines and growth factors, such as factors involved in inflammation (*i.e.*, MCP-1, M-CSF, IL-8), angiogenesis (*i.e.*, VEGF- α) and tissue remodelling (*i.e.*, MMP-13, OPG) [10,11].

Cell type is an essential factor determining ECM composition. Cells derived from different tissues typically yield matrices that mimic the composition of its natural tissue matrix [12]. Decellularized ECM from mesenchymal stem/stromal cells (MSC) and human umbilical vein endothelial cells (HUVEC) have been shown to promote MSCs proliferation and osteogenic differentiation [13,14]. Moreover, recent research has focused on the use of co-culture systems and co-cultured MSCs and HUVECs were shown to enhance osteogenic differentiation of MSCs. For instance, endothelial cells secrete factors, such as bone morphogenetic proteins (BMPs) [15] that are beneficial for osteogenic differentiation of MSCs [16]. The optimal cell ratio in co-cultures of human MSC and HUVEC is still under investigation, however, a 1:1 ratio was reported to be optimal for both osteogenesis and angiogenesis [17]. To cope with this and with the advantage of affording a more reliable bone niche *in vivo*, we produced ECM derived from co-cultured MSCs and HUVECs, expecting to enhance the proliferation and osteogenic differentiation of MSCs.

Decellularized ECM have shown improvements in biological activity, however, their mechanical properties are still insufficient to support and regenerate hard tissues such as bone [18,19]. Therefore, cell-derived ECM can be combined with synthetic biomaterials to improve the mechanical properties and enhance cell-material interactions. In particular, electrospinning has been often used to fabricate fibrous and porous scaffolds from a variety of natural and synthetic materials for a broad range of tissue engineering applications [20–23]. Moreover, the high surface area, porosity and interconnectivity of the electrospun fibers are favorable for cell attachment and proliferation and also facilitate nutrient supply and waste removal [20,22]. Electrospun fibers are highly relevant for bone tissue engineering due to the fact that their architecture mimics the hierarchical organized micro/nano scale fibrous structure found in the native bone ECM [24].

Polycaprolactone (PCL) is a FDA-approved, biodegradable and biocompatible synthetic material that has been extensively used in biomedical applications [25]. Due to its semi-crystalline and hydrophobic nature, PCL has a slow degradation rate and mechanical properties suitable for different tissue engineering settings, with special relevance in repairing defects in hard and slow regenerating tissues like bone [26–29]. Accordingly, PCL electrospun fibrous scaffolds were previously used in bone repair either in their pristine form or in different coupled strategies to improve scaffold osteoinductive capacity. Such coupled strategies include fiber surface modification with bioactive coatings or immobilized biomolecules, or blending with other copolymers [22,30–34].

3D cell-derived ECM scaffolds have been developed in combination with different organic and inorganic materials. Cell-derived ECM - PCL scaffolds [35], - titanium implants [36] and - hydroxyapatite scaffolds [37] have been applied in bone repair and demonstrated enhancement

of cell proliferation and osteogenic differentiation. Recent approaches include combinations of cell-derived ECM with electrospinning techniques to develop scaffolds that mimic not only the architecture and structure of ECM, but also its composition [38–41]. These scaffolds have shown superior mechanical properties and maintenance of bioactivity in various tissue engineering applications [42–44]. Different approaches have been applied to bone tissue engineering applications. Gibson and co-workers incorporated decellularized ECM nanoparticles from bone into a biosynthetic nanofiber composite scaffold [45] while Jeon and colleagues have cultured pre-osteoblasts on electrospun PCL scaffolds and decellularized it to obtain decellularized cell-derived ECM scaffolds [39]. Most of the studies reported in the literature developed strategies to decorate electrospun nanofibers with ECM by seeding cells onto the fibers, allowing them to grow followed by decellularization to obtain the ECM-decorated electrospun fibers. A different approach has also emerged in which the cell-derived ECM is produced in regular *in vitro* cell culture dishes, collected and lyophilized to generate ECM powder that can be added to the polymer solution and electrospun to generate fibers with incorporated cell-derived ECM particles [41]. Accordingly, we expected that by directly incorporating cell-derived ECM into PCL electrospun fibers, we could develop hybrid bioactive scaffolds with the appropriate structural and mechanical support using a synthetic material and ECM-mediated signaling to target different cellular processes, such as proliferation, osteogenic differentiation and angiogenesis.

The aim of this study was to develop cell-derived ECM PCL electrospun scaffolds derived from different cell sources: MSCs, HUVEC and co-culture of MSC:HUVEC and test their potential in bone regeneration. The scaffolds were characterized in terms of their structural, thermal and mechanical properties. Their ability to support MSCs osteogenic differentiation was evaluated by assessing cell proliferation, biochemical activity and gene expression. To our knowledge, this is the first study in which ECM derived from a co-culture of MSCs and HUVECs was incorporated into PCL electrospun fibers to develop a bioactive scaffold targeting bone repair applications.

2. Materials and methods

2.1. Cell culture

Human bone marrow MSCs were obtained from Lonza (Basel, Switzerland). Human bone marrow MSCs were thawed and plated on T-75 cm² flasks using low-glucose Dulbecco's Modified Eagle Medium (DMEM, Gibco, Grand Island, NY) supplemented with 10% fetal bovine serum (FBS, Gibco) and 1% penicillin-streptomycin (Pen-strep, Gibco) and kept at 37 °C and 5% CO₂ in a humidified atmosphere. HUVECs were purchased from Lonza and maintained in commercial endothelial growth medium-2 (EGM-2, Lonza) and kept at 37 °C, 5% CO₂ in a humidified atmosphere. Medium renewal was performed every 3–4 days. All the experiments were performed using cells between passages 3 and 5.

2.2. Decellularized cell-derived ECM preparation and characterization

MSCs, HUVECs and co-culture of MSC:HUVEC (1:1) were seeded at 5000 cells/cm². MSCs were incubated with DMEM + 10% FBS + 1% Pen-strep, HUVECs with EGM-2 growth medium and co-culture of MSC:HUVEC was cultured in a combination of DMEM + 10% FBS + 1% Pen-strep and EGM-2 (1:1). Cells were expanded for 7–10 days and medium was replaced every 3–4 days. After reaching confluency, medium was discarded and cells were washed in phosphate buffered saline (PBS, Gibco). Based on previously reported methods [14,46], ECM isolation was performed by a decellularization protocol using a 20 mM ammonium hydroxide (NH₄OH) + 0.5% Triton X-100 (Sigma-Aldrich, St. Louis, MO) solution. The solution was added to the culture and incubated for 5 min at room temperature. After microscopic

confirmation of complete cell lysis and presence of intact ECM on the surface of the wells, ECM was gently washed 3 times with distilled water. ECM layer was detached from the well using a cell scraper and collected in falcon tubes. The different cell-derived ECM powders to be further used in electrospinning procedure were obtained after freeze-drying.

The ECM protein components and distribution pattern of the different decellularized cell-derived ECM were evaluated by immunofluorescent staining of collagen I, fibronectin and laminin. Therefore, upon decellularization, cell-derived ECM were washed with PBS and fixed with 4% (v/v) paraformaldehyde (PFA: Santa Cruz Biotechnology, Dallas, TX, USA) for 20 min at room temperature. After washing three times with 1% bovine serum albumin (BSA, Sigma) in PBS, samples were blocked with a solution of 0.3% Triton X-100, 1% BSA and 10% donkey serum (Sigma) in PBS for 45 min at room temperature. Primary antibodies including mouse anti-human collagen I, fibronectin and laminin (R&D Systems, 10 $\mu\text{g}/\text{mL}$ in a solution of 0.3% Triton X-100, 1% BSA, 10% donkey serum in PBS) were added into the samples and incubated overnight at 4 °C. After washing once with PBS, a NorthernLights™ 557-conjugated anti-mouse IgG secondary antibody (R&D Systems, dilution 1:200 in 1% BSA, PBS) was added into the samples and incubated for 1 h at room temperature and protected from light. The fluorescent staining was imaged by fluorescence microscope (Olympus IX51 Inverted Microscope: Olympus America Inc., Melville, NY) and recorded by an attached digital camera.

2.3. Fabrication of cell-derived ECM electrospun PCL fibers

Poly (ϵ -caprolactone) (PCL, $M_n = 80,000$ Da, Sigma-Aldrich) was dissolved at 11% w/v in 1,1,1,3,3,3-hexafluoro-2-propanol (HFIP, Sigma-Aldrich) under agitation overnight at room temperature. Based in a previous study performed by Thakkar et al. [41], lyophilized cell-derived ECM was incorporated into the PCL solution (0.25 mg/mL) followed by agitation overnight to produce a final homogeneous solution of PCL 11% w/v-0.025% w/v ECM (in HFIP). The fibrous scaffolds were fabricated by electrospinning. PCL-ECM solution (5 mL) was loaded into a syringe placed in a pump and connected to a PTFE tube, which was attached on the other end to a 21G metallic needle (0.8 mm diameter). A controlled flow rate of 3 mL/h and an applied voltage of 20 kV were used, creating a potential difference between the needle and a grounded aluminum foil collector placed at a distance of 21 cm from the needle tip. The different PCL-ECM electrospun fiber mats were produced under the same process parameters and ambient conditions (temperature and relative humidity varied between 19 and 21 °C and 20–25%, respectively) for approximately 60 min to ensure scaffold thickness. An overview of the procedure to fabricate cell-derived ECM microfibrillar scaffolds is presented in Scheme 1.

2.4. Characterization of cell-derived ECM electrospun scaffolds

2.4.1. Scanning electron microscopy (SEM) analysis

The morphological and structural characterization of the lyophilized cell-derived ECM powders and PCL-ECM electrospun fibers was performed using a field emission scanning electron microscope (FE-SEM, FEI-Versa 3D Dual Beam, Hillsboro). Prior to imaging, samples were mounted on a holder and sputter-coated with a thin layer of 60% gold-40% palladium. Samples were imaged at several magnifications using an accelerating voltage of 2–3 kV. The average fiber diameters and subsequent distributions of PCL-ECM electrospun scaffolds were determined by measuring 100 individual fibers per condition from at least 5 different SEM images using ImageJ software (ImageJ 1.51f, National Institutes of Health, USA).

2.4.2. Picro-sirius red staining

Picro-sirius red stain kit (Abcam, Cambridge, MA) was used to identify collagen components on the PCL-ECM electrospun scaffolds, following the manufacturer's guidelines. Briefly, scaffolds were washed with PBS and incubated with Picro-sirius red solution for 60 min. The samples were rinsed twice with acetic acid solution, once with absolute ethanol and washed three times with PBS. Scaffolds were imaged using a bright field microscope (Olympus IX51 Inverted Microscope, NY USA).

2.4.3. FTIR analysis

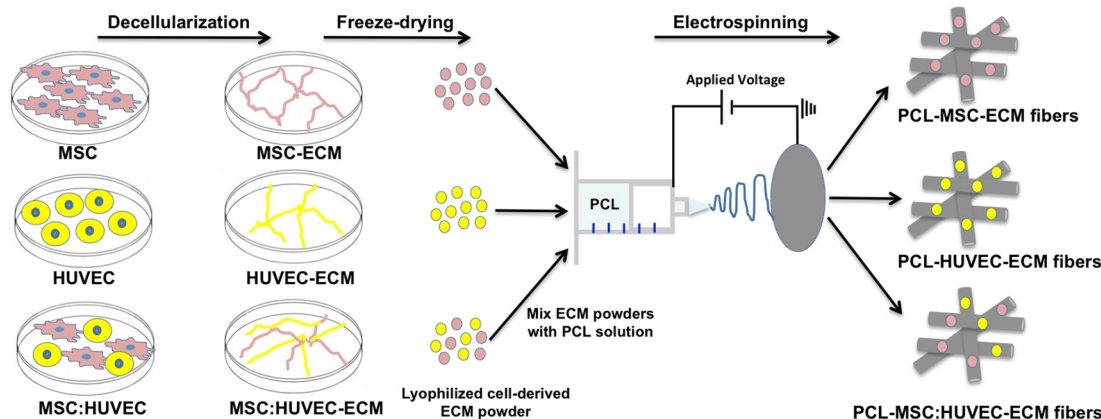
Fourier transform infrared (FTIR) (Perkin Elmer Spectrum One FT-IR Spectrometer, USA) was used to identify the functional groups of the different lyophilized cell-derived ECM powder and fibrous scaffolds. Powder cell-derived ECM samples were mixed with potassium bromide (KBr) in pellets before the analysis in transmission mode in the spectral region of 4000–450 cm^{-1} and a resolution of 4 cm^{-1} . Attenuated total reflectance (ATR-FTIR) mode was used to obtain the spectra of the different cell-derived ECM electrospun scaffolds collected between the spectral region 4000–650 cm^{-1} and a resolution of 4 cm^{-1} .

2.4.4. Differential scanning calorimetry (DSC) analysis

Pre-weighed samples were hermetically sealed in aluminum pans and subjected to heating and cooling cycles between –50 °C and 100 °C at a constant heating rate of 5 °C/min using a TA Instruments DSC-Q100 apparatus (New Castle, Delaware, USA). Universal Analysis software V4.7A (TA Instruments) was used for data analysis to determine melting and crystallization temperatures.

2.4.5. Mechanical tensile testing

Mechanical properties of cell-derived ECM electrospun scaffolds were tested under uniaxial tensile testing using a mechanical tester (Instron® Model 5843) with a 10 N load cell and a constant



Scheme 1. A scheme of the experimental procedure for the fabrication of cell-derived ECM microfibrillar scaffolds.

displacement rate of 10 mm/min. Five different test specimens ($N = 5$) for each condition were prepared in a rectangular shape with a length of 15 mm, width of 10 mm and a thickness of 0.1 mm. Experimental data was collected and processed using the Bluehill® 2 software. The Young's modulus was determined from the slope of the initial linear strain region (0–15%) of the stress-strain curve. Ultimate tensile strength (UTS) and ultimate elongation were also obtained from the stress-strain curves.

2.5. Cell culture on cell-derived ECM electrospun scaffolds

Prior to cell culture, cell-derived ECM electrospun scaffolds were sterilized by UV exposure for 4 h, placed in ultra-low cell attachment 24-well plates and washed three times with PBS + 1% Pen-Strep solution. Then, scaffolds were soaked in culture medium and incubated at 37 °C for 1 h.

Human bone marrow MSCs were seeded on the different types of cell-derived ECM electrospun PCL scaffolds at a density of 50,000 cells per scaffold and incubated for 2 h at 37 °C and 5% CO₂ to allow cell attachment. Osteogenic medium composed by DMEM supplemented with 10% FBS, 10 mM β-glycerophosphate (Sigma-Aldrich), 10 nM dexamethasone (Sigma-Aldrich), 50 μg/mL ascorbic acid (Sigma-Aldrich) and 1% Pen-strep was added to all the scaffolds. The metabolic activity of MSCs was evaluated using AlamarBlue® cell viability reagent (ThermoFischer Scientific, USA) on days 3, 7, 14 and 21 following the manufacturer's guidelines. Briefly, a 10% (v/v) AlamarBlue® solution in culture medium was added to the scaffolds and incubated at 37 °C in 5% CO₂ chamber for 3 h. Fluorescence intensity was measured in a microplate reader (SpectraMax M5, Molecular Devices, USA) at an excitation/emission wavelength of 560/590 nm and compared to a calibration curve to assess the number of cells in each scaffold. Four scaffolds were used for each condition and fluorescence was measured in triplicates.

Cells were washed twice with PBS, fixed with 4% PFA for 20 min and then permeabilized with 0.1% Triton X-100 for 10 min to assess cell morphology. After permeabilization, cells were incubated with Phalloidin-TRITC (Sigma-Aldrich) (dilution 1:250, 2 μg/mL) for 45 min in the dark. Cells were then washed twice with PBS, counterstained with DAPI (Sigma-Aldrich, 1.5 μg/mL) for 5 min and washed with PBS. The fluorescent staining was imaged using a fluorescence confocal microscope (Leica STED TCS SP8 3×, Wetzlar, Germany). Cell morphology along the culture (days 7, 14 and 21) was also analyzed using SEM (see Section 2.4.1). Fixed cells were stained with 1% (v/v) osmium tetroxide (Sigma-Aldrich) solution for 30 min and washed twice with PBS. After, samples were dehydrated using ethanol gradient solutions (20%, 40%, 60%, 80%, 95% and 100% (v/v)) and finally dried in a critical point dryer (supercritical Automegasamdri 915B, Tousimis, USA) in 100% isopropanol.

2.6. Assessment of MSCs osteogenic differentiation on cell-derived ECM electrospun scaffolds

2.6.1. ALP activity assay

After 14 and 21 days of osteogenic differentiation, alkaline phosphate (ALP) activity was detected using a colorimetric ALP kit (BioAssays Systems, Hayward, CA) according to the manufacturer's protocol. Samples were washed with PBS and were incubated in the lysis buffer (0.1% Triton X-100 in PBS) overnight at room temperature. The lysate was added to *p*-nitrophenyl phosphate solution (10 mM) provided with the ALP kit. The absorbance was measured on a plate reader (SpectraMax M5, Molecular Devices, USA) at 405 nm and normalized to the total number of cells in each scaffold. Three different scaffolds were used for each condition and absorbance was measured in triplicates.

2.6.2. Calcium assay

Calcium content quantification was determined after 14 and 21 days of MSCs osteogenic differentiation on cell-derived ECM electrospun scaffolds. Samples were washed with PBS and incubated with a 0.5 M HCl solution (Sigma-Aldrich) with agitation overnight at 4 °C. The supernatant was used for calcium determination according to the manufacturer's instructions in the calcium colorimetric assay kit (Sigma-Aldrich). Total calcium was calculated from a calcium standard solution prepared in parallel. Absorbance at 575 nm was measured for each condition on a plate reader (SpectraMax M5, Molecular Devices, USA) and normalized to the total number of cells. Three scaffolds were used for each condition and absorbance values were measured in triplicates.

2.6.3. Osteogenic staining

After 21 days of osteogenic differentiation, samples were assessed using Alizarin Red, ALP/Von Kossa and Xylenol orange staining. Cell culture medium was removed and samples were washed once with PBS, and fixed with 4% PFA for 20 min. Then, scaffold samples were stained with a 2% Alizarin red solution (Sigma-Aldrich) by incubation for 1 h at room temperature. After, the scaffolds were washed three times with miliQ water and imaged (Olympus IX51 Inverted Microscope, NY USA). For ALP staining, samples were rinsed in miliQ water during 5 min and incubated with Fast Violet solution (Sigma-Aldrich) and Naphthol AS-MX Phosphate Alkaline solution (Sigma-Aldrich) in a final concentration of 4% for 45 min at room temperature in the dark. In the case of Von Kossa staining, the same scaffold samples used for ALP staining were washed twice with miliQ water and incubated with 2.5% silver nitrate solution (Sigma-Aldrich) for 30 min at room temperature protected from light. Finally, samples were washed three times with miliQ water and observed under the microscope. To further confirm the presence of mineral deposits formed after MSCs osteogenic differentiation on cell-derived ECM electrospun scaffolds, a 20 mM Xylenol orange solution (Sigma-Aldrich) was added to previously fixed samples and incubated for 1 h at room temperature in the dark. After that, scaffolds were washed with miliQ water, counterstained with DAPI (Sigma-Aldrich) (1.5 μg/mL) for 5 min and washed with PBS. The fluorescent staining of the produced minerals was observed by fluorescence microscopy (Olympus IX51 Inverted Microscope, NY USA).

2.6.4. Energy dispersive X-ray (EDX) analysis

Carl Zeiss Supra field emission scanning electron microscope (FESEM, Hillsboro, USA) was used to conduct energy dispersive x-ray spectroscopic (EDX) analysis on the scaffolds after 21 days of MSCs osteogenic differentiation. Analysis was performed with an acceleration voltage of 10 kV and a spot size of 120 μm. The presence of mineral elements on the EDX spectra of each sample was analyzed using INCA Microanalysis Suite software.

2.6.5. RNA extraction and quantitative real-time PCR analysis

Total RNA was extracted using the RNeasy Mini Kit (QIAGEN, Hilden, Germany). Briefly, the scaffolds were first incubated in lysis buffer with 200 rpm agitation for 1 h at 4 °C. Afterwards, total RNA was isolated according to the manufacturer's protocol and quantified using a Nanodrop (ND-1000 Spectrophotometer, Nanodrop Technologies). cDNA was synthesized from the purified RNA using iScript™ Reverse Transcription Supermix (Bio-Rad, Hercules, CA USA) according to manufacturer's guidelines. Reaction mixtures (20 μL) were incubated in a thermal cycler (Veriti Thermal Cycler, Applied Biosystems, CA USA) for 5 min at 25 °C, 20 min at 46 °C and 1 min at 95 °C and then were maintained at 4 °C.

The quantitative reverse transcription-polymerase chain reaction (qRT-PCR) was performed using PowerUp SYBR® Green Master Mix (Applied Biosystems) and StepOnePlus real-time PCR system (Applied Biosystems). All reactions were carried out at 95 °C for 10 min, followed by 40 cycles of 95 °C for 15 s and 60 °C for 1 min. All samples were analyzed in triplicate. Results were analyzed using the 2^{-ΔΔC_t} method to

Table 1
Forward and reverse primer sequences used in qRT-PCR analysis.

Gene	Primer sequences
<i>GAPDH</i>	Fwd: 5'-AACAGCGACACCCACTCCTC-3' Rev: 5'-CATACCAGGAAATGAGCTTGACAA-3'
<i>Runx2</i>	Fwd: 5'-AGATGATGACACTGCCACTCTG-3' Rev: 5'-GGGATGAAATGCTTGGAAC-3'
<i>ALP</i>	Fwd: 5'-ACCATTCCACGTCTTCACATT-3' Rev: 5'-AGACATTCTCTCGTTCACCGCC-3'
<i>OPN</i>	Fwd: 5'-TGTGAGGTGATGCTCGTCTGTAG-3' Rev: 5'-ACACATATGATGGCCGAGGTGA-3'
<i>VEGF</i>	Fwd: 5'-TGCCTCAGAAGAGCTGAAAC-3' Rev: 5'-CACAGACTCCCTGCTTTTGTCT-3'

determine relative changes in target osteogenic marker gene expression as compared to controls. Target gene expression was primarily normalized to the housekeeping gene glyceraldehyde 3-phosphate dehydrogenase (*GAPDH*) and then determined as a fold-change relative to the baseline expression of target gene measured in MSCs at day 0 (prior to scaffold seeding). Primer sequences used in the qRT-PCR analysis are presented in Table 1.

2.7. Statistical analysis

Each experiment was conducted in triplicate, unless specified differently. The statistical analysis of the data was performed using one-way ANOVA, followed by Tukey post-hoc test. GraphPad Prism version 6 software was used in the analysis and data was considered to be significant when *p*-values obtained were < 0.05 (95% confidence intervals, **p* < 0.05).

3. Results

3.1. Lyophilized cell-derived ECM characterization

Microstructural features were observed under SEM microscopy from lyophilized cell-derived ECM powders of different cell types including MSCs, HUVECs and co-culture of MSC and HUVEC (Supplementary Fig. S1a). All the lyophilized ECM produced from different cell types demonstrated similar patterns with a rugged surface. FTIR spectra of lyophilized ECM derived from different cell types, such as MSCs, HUVECs and MSC:HUVEC showed different infrared peaks (Supplementary Fig. S1b). Notably, FTIR spectra of lyophilized MSC:HUVEC ECM demonstrated infrared peaks corresponding to peaks present only in MSC ECM and HUVEC ECM spectra exclusively, indicating the presence of components from both types of ECM.

The different types of cell-derived ECM prepared were also assessed for the presence and distribution of major ECM components by immunocytochemistry (Supplementary Fig. S2). Interestingly, despite immunocytochemistry analysis demonstrated that all types of ECM stained positive for collagen type I, a more intense staining was clearly observed in the ECM types generated by MSC (MSC-ECM and MSC:HUVEC-ECM). Moreover, the expression of laminin and fibronectin from the different decellularized cell-derived ECM presented different intensity and distribution patterns. In fact, MSC:HUVEC ECM demonstrated a more intense signal of laminin and fibronectin compared to MSC ECM and HUVEC ECM. Additionally, HUVEC-ECM expressed relatively lower levels of laminin, in the form of a sparse dot-like morphology compared to the other cell-derived ECM.

3.2. Cell-derived ECM electrospun scaffold characterization

SEM micrographs of MSC ECM, HUVEC ECM and MSC:HUVEC ECM PCL electrospun fibers and PCL scaffold without ECM (used as a control) showed that all the scaffolds were highly porous with high

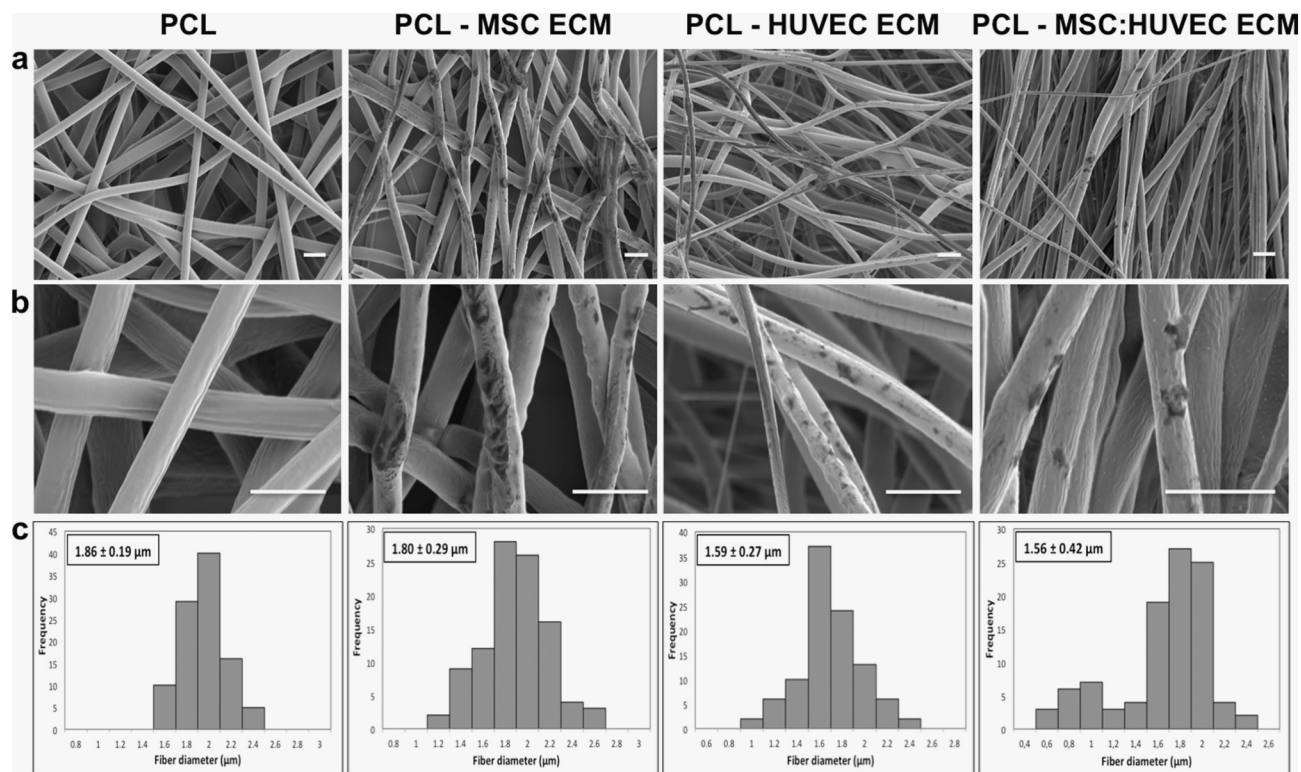


Fig. 1. SEM micrographs at lower magnification to provide a broad view of the scaffold (a) and at a higher magnification (b) of PCL and different cell-derived ECM PCL electrospun scaffolds fabricated. Fiber diameter distribution histograms (c) of PCL and the different cell-derived ECM PCL electrospun scaffolds. Scale bar 5 μm.

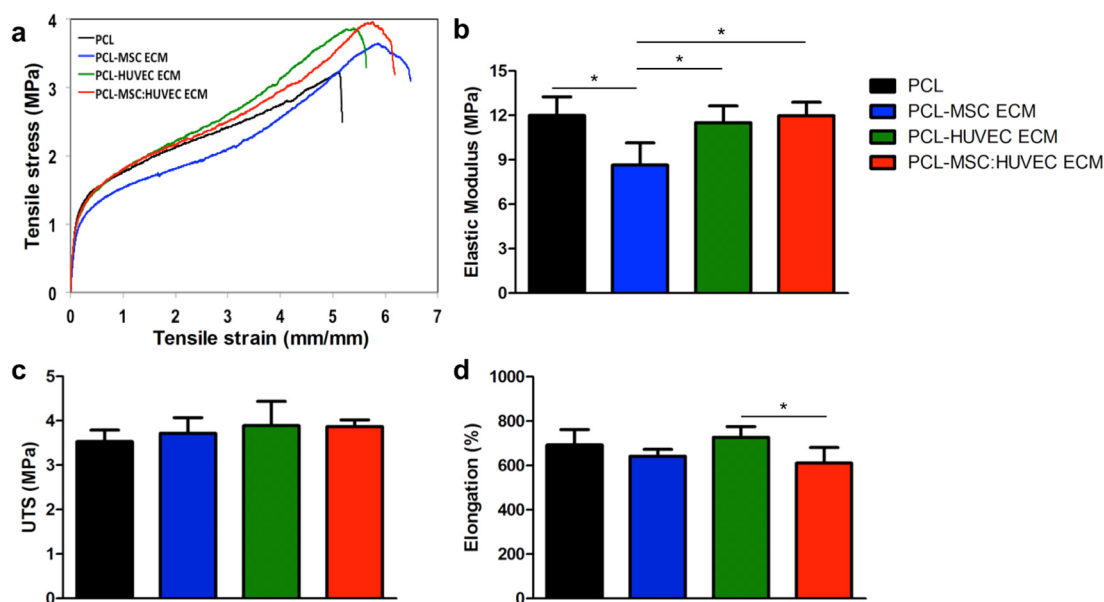


Fig. 2. Mechanical properties of cell-derived electrospun scaffolds obtained after tensile testing: Representative stress-strain curves (a), elastic modulus (b), ultimate tensile strength (UTS) (c) and ultimate elongation (d). Five different samples ($N = 5$) were used in the analysis; $*p < 0.05$.

interconnectivity and micro/nanoscale structural features. Interestingly, ECM particles were clearly detectable in all the cell-derived ECM electrospun fibers as verified under SEM microscopy analysis (Fig. 1a,b). Furthermore, all the fabricated scaffolds were composed mainly of microfibers. The average fiber diameter of electrospun PCL without ECM was $1.86 \pm 0.19 \mu\text{m}$ whereas MSC ECM, HUVEC ECM, MSC:HUVEC ECM PCL electrospun scaffolds demonstrated an average fiber diameter of $1.80 \pm 0.29 \mu\text{m}$, $1.59 \pm 0.27 \mu\text{m}$ and $1.56 \pm 0.42 \mu\text{m}$, respectively. Therefore, all the electrospun fibers presented similar diameters at the microscale, indicating that the incorporation of cell-derived ECM into the PCL casting solution did not greatly impact the electrospinning process and the average fiber diameter of scaffolds (Fig. 1c). Cell-derived ECM scaffolds stained positive with Picro-sirius red, validating the presence of collagens. On the other hand, no collagen presence was observed in the PCL scaffolds without ECM incorporated (Supplementary Fig. S3).

Analysis of the mechanical properties of cell-derived ECM PCL scaffolds demonstrated that the incorporation of ECM into the PCL solution did not drastically affect the mechanical properties of the microfibrous scaffold, as shown by the representative stress-strain curves (Fig. 2a) and by the elastic modulus, UTS and elongation values (Fig. 2b, c, d and Supplementary Table 1). PCL alone, MSC ECM, HUVEC ECM and MSC:HUVEC ECM PCL electrospun fibers presented values for elastic modulus of $11.99 \pm 1.26 \text{ MPa}$, $8.65 \pm 1.49 \text{ MPa}$, $11.50 \pm 1.15 \text{ MPa}$ and $11.98 \pm 0.92 \text{ MPa}$, respectively. Average values for UTS and elongation are also summarized in the Supplementary Table 1. Interestingly, only the PCL-MSCECM fibers presented a statistically significant decrease in the elastic modulus compared to all the other conditions.

ATR-FTIR spectrum of PCL electrospun scaffold showed all the major characteristic IR peaks of PCL at approximately 1724 and 1160 cm^{-1} that correspond to ester carbonyl bond stretching and carbon-oxygen bond stretching, respectively. The IR spectra of the cell-derived ECM PCL electrospun scaffolds appeared to have an identical pattern to PCL but did not show any major peaks that correspond to ECM (see Supplementary Fig. S1b). This is probably due to the low amount of ECM present in the PCL-ECM scaffolds compared to the large amount of PCL (Supplementary Fig. S4).

Thermal analysis of cell-derived ECM electrospun scaffolds was performed using differential scanning calorimetry (DSC). DSC

thermograms of cell-derived ECM electrospun scaffolds are shown in Supplementary Fig. S5. PCL fibers showed characteristic endothermic (melting) and exothermic (crystallization) transformation points at around 57.7°C (Supplementary Fig. S5a) and 36.2°C (Supplementary Fig. S5b), respectively. Thermograms of all the other samples containing the different cell-derived ECM are similar to the neat PCL fibers. The presence of ECM has no significant effect on the average phase transition temperatures of the composite fibers. There are slight decrements in the melting and crystallization points that can be accounted to experimental and instrumental variability.

3.3. Effects of cell-derived ECM electrospun scaffolds on cell proliferation

Metabolic activity of MSCs was measured by AlamarBlue® assay on days 3, 7, 14 and 21 to assess the effect of the different cell-derived ECM electrospun scaffolds on cell proliferation (Fig. 3a). Notably, after 7 days, a significant increase in cell number was found on all cell-derived ECM scaffolds compared to PCL scaffolds alone, which was also observed in the subsequent time points of the culture (days 14 and 21) (Fig. 3a). The cell number increase, shown in Fig. 3a, suggests a beneficial MSCs response to the presence of ECM in the microfibers. Although all cell-derived ECM scaffolds significantly enhanced cell proliferation when compared to PCL scaffold, no significant differences were observed between the ECM derived scaffolds generated from different cell sources. The morphology of cells cultured in the different cell-derived ECM PCL electrospun scaffolds was assessed at the end of the culture by DAPI-Phalloidin staining (Fig. 3b). Fig. 3b shows MSCs morphology, distribution and organization throughout the electrospun scaffolds after 21 days of osteogenic differentiation. Cells seeded on all the scaffolds (with and without ECM) presented similar morphology, however a higher cell spreading and scaffold population in cell-derived ECM electrospun scaffolds is suggested by the observation of Fig. 3b. SEM analysis throughout the culture at days 7, 14 and 21 (Supplementary Fig. S6) is consistent with the results from cell proliferation assay. Cell-derived ECM PCL microfibrous scaffolds were already highly populated with MSCs at day 7, which was not observed for the PCL only scaffold.

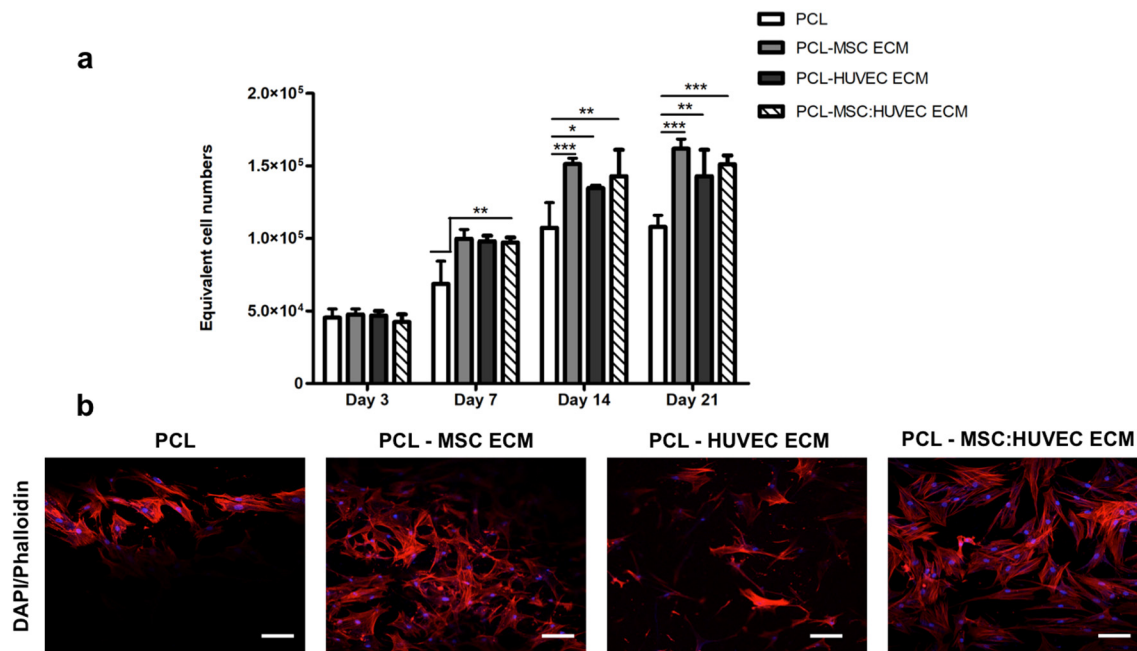


Fig. 3. Effects of cell-derived electrospun scaffolds on MSCs proliferation. Cell proliferation assay (a) and cell morphology assessment by DAPI-Phalloidin staining at day 21 (b). Values are expressed as mean \pm SD ($N = 4$); * $p < 0.05$, ** $p < 0.01$, *** $p < 0.001$; scale bar 100 μm .

3.4. Influence of cell-derived ECM electrospun PCL fibers on osteogenic differentiation

MSCs cultured on cell-derived ECM scaffolds presented higher ALP activity values compared to PCL only scaffolds, after 14 days of differentiation. However, this enhancement in ALP activity was only statistically significant when cells were cultured in PCL-MSC:HUVEC ECM scaffolds. After 21 days, the ALP activity of MSCs cultured on all electrospun scaffolds decreased, presenting similar results to the ones verified for PCL alone (Fig. 4a).

Regarding mineralization, no drastic differences were observed between the scaffolds after 14 days of differentiation. However, after 21 days of osteogenic differentiation, a statistically significant enhancement in calcium accumulation was only observed when MSCs were seeded on PCL-HUVEC ECM scaffold compared to the other cell-derived electrospun scaffolds (Fig. 4b).

The most common methods to visualize *in vitro* mineralization are the ALP/Von Kossa, Alizarin red and Xylenol orange staining. Alizarin red staining (Fig. 4c, top) confirmed the presence of calcium deposits in all scaffolds after 21 days of osteogenic differentiation, validating the results obtained with calcium deposition quantification. Moreover, ALP/Von Kossa staining also confirmed ALP activity in all scaffolds (reddish areas), as well as, indirectly, the presence of calcium deposits (darker regions highlighted by the white arrows) (Fig. 4c, middle), demonstrating the successful differentiation of MSCs into osteoblasts in all PCL scaffolds. Xylenol orange fluorescent staining further confirmed the presence of calcium deposits on MSCs cultured on all cell-derived ECM PCL electrospun scaffolds and PCL fibers after 21 days of osteogenic differentiation (Fig. 4c, bottom).

SEM micrographs showed MSCs attached to the fibers and detected some ECM produced and deposited by cells surrounding the fibers (Fig. 5a). Additionally, elemental analysis of MSCs differentiated for 21 days on cell-derived ECM scaffolds further confirmed the presence of calcium and phosphorous (Fig. 5b).

3.5. Gene expression analysis

Different osteogenic marker genes were analyzed (*Runx2*, *ALP* and *OPN*), as well as the angiogenic marker gene *VEGF* (Fig. 6).

Interestingly, all the scaffolds (with and without ECM) upregulated the expression of *Runx2* (Fig. 6b) and *OPN* (Fig. 6c) compared to the control (cells at day 0). Regarding *Runx2* and *ALP* (Fig. 6a) gene expression, PCL-MSC:HUVEC ECM demonstrated a statistically significant increase compared to all the other experimental groups. Additionally, cells cultured on PCL-MSC:HUVEC ECM electrospun scaffolds presented higher *OPN* expression levels than all the other scaffolds. Such increase in *OPN* expression was only statistically significant when compared to PCL-HUVEC ECM and PCL only scaffolds. In contrast, *VEGF* (Fig. 6d) gene expression levels were only significantly enhanced comparing to PCL when cells were cultured in PCL-HUVEC ECM scaffolds. Although a slight increase in *VEGF* expression was also observed in PCL-MSC ECM and PCL-MSC:HUVEC ECM groups comparing to PCL, such differences were not considered statistically significant.

4. Discussion

Cell-derived ECM can be used as an alternative approach to obtain scaffolds with complexity closer to native tissue microenvironment and with enhanced bioactivity. For this, cells were cultured *in vitro* until confluence and allowed to secrete ECM. Afterwards, a decellularization treatment is used to remove the cellular components, while retaining the ECM structure. Different studies have already reported the effects of cell-derived ECM on cellular activities by combining it into scaffolds [39,41]. In particular, for bone tissue engineering applications, Gibson and colleagues fabricated a PCL electrospun scaffold incorporated with decellularized ECM nanoparticles from bone, demonstrating upregulation of osteogenic gene expression markers [45]. Moreover, Jeon and colleagues have cultured pre-osteoblasts on electrospun PCL scaffolds and decellularized it to obtain decellularized cell-derived ECM scaffolds, improving cell proliferation and osteogenic differentiation [39]. However, most of these studies use cell-derived ECM as a coating strategy to decorate the scaffold. Thus, cells are cultured and allowed to grow on top of the scaffolds and upon application of the decellularization treatment, the ECM components remain attached to the scaffold. Notably, in this current study, we used a different approach to fabricate cell-derived ECM PCL scaffolds. Here, cell-derived ECM, produced from different cell types relevant for bone homeostasis, was obtained after culturing them *in vitro* and collecting the secreted ECM upon

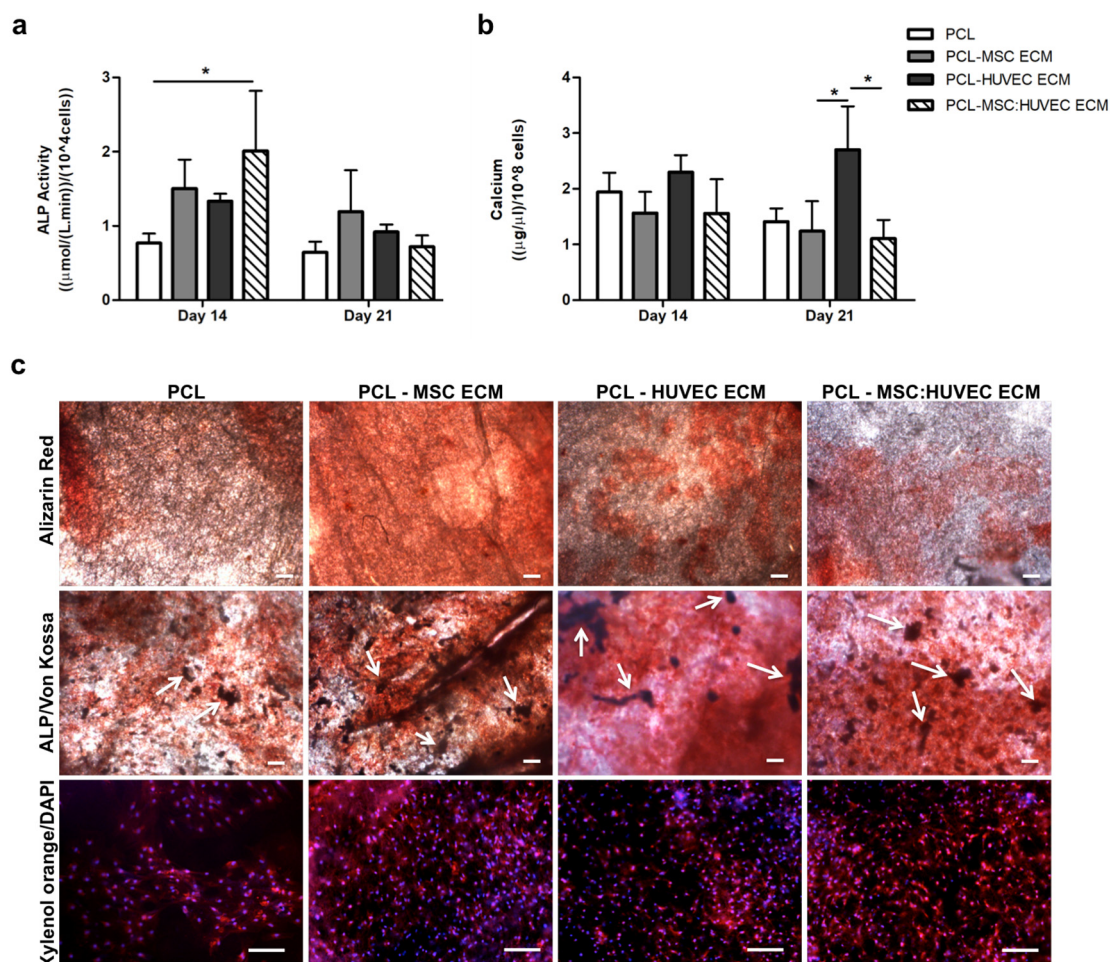


Fig. 4. Osteogenic differentiation of MSCs cultured on cell-derived ECM electrospun fibers. ALP activity (a) of MSCs cultured on cell-derived ECM PCL scaffolds after 14 and 21 days of osteogenic differentiation. Calcium deposition quantification (b) of MSCs seeded on cell-derived ECM PCL scaffolds after 14 and 21 days of osteogenic differentiation. Alizarin red, ALP/Von Kossa and Xylenol Orange stainings of MSCs differentiated on cell-derived ECM scaffolds after 21 days (c). Alizarin red staining confirmed the presence of calcium deposits (reddish areas). ALP/Von Kossa staining demonstrated ALP activity of MSCs cultured on all PCL scaffolds (reddish areas) and the presence of mineralized deposits (Von Kossa – darker areas, as highlighted by the white arrows). Xylenol Orange fluorescent staining confirmed the presence of calcium deposits. DAPI was used to counterstain the cell nuclei in blue. Scale bar, 200 μm. Values are expressed as mean ± SD (N = 3); *p < 0.05. (For interpretation of the references to colour in this figure legend, the reader is referred to the web version of this article.)

application of a previously reported decellularization method [14,46]. Afterwards the obtained ECM was collected and lyophilized. The lyophilized ECM was then directly mixed into the PCL solution and electrospinning technique was used to produce cell-derived ECM PCL microfibrous scaffolds. It has been previously reported that ECM lyophilization leads to water removal and drying of the biologically active component contained in it, making the ECM proteins more stable [47].

Due to tissue specificity, cell source is known to be a determining factor for the composition of the cell-derived ECM. Indeed, cells derived from different tissues typically produce matrices that will recreate the composition of the natural tissue matrix [12]. Therefore, taking into account the native bone microenvironment, in this study we fabricated cell-derived ECM PCL scaffolds, composed with ECM derived from MSCs, HUVECs and a co-culture of MSC:HUVEC. In fact, co-culture of MSCs and endothelial cells has demonstrated extensive cellular cross-talk, enhancing the angiogenic response of MSCs [48,49], as well as the osteogenic capabilities [15]. However, the optimal cell ratio in co-cultures of human MSC and endothelial cells is still under investigation and data on optimal culture conditions of co-cultures of MSC and endothelial cells are still lacking, specifically taking into consideration osteogenic and angiogenic properties. Notably, Ma and colleagues tested several MSC/endothelial cells ratios and observed improved

osteogenesis and angiogenesis when a MSC/HUVEC 1:1 ratio was used [17]. Consequently, in this study, the cell-derived ECM was generated from MSCs, HUVECs and one of their combination (1:1) and emphasis was placed on the biological activities of these cells and the characterization of the resultant matrix. It is known that the basic molecules constituting ECM may be similar in all organisms, but their distribution and organization varies with species, tissue type, age or physiological state of the host [50]. Therefore, cell-derived ECM generated from different cell types may present differences in their composition and these structural differences may induce different cellular responses when used as scaffolds for tissue engineering. Future studies should focus on identifying the composition of each ECM-type using proteomics/glycomics analysis.

Here, lyophilized ECM powders derived from different cell types and their co-culture were characterized by SEM and FTIR (Supplementary Fig. S1). Results showed that morphology of the different cell-derived ECM was similar between the different cell types and co-culture and consistent with other lyophilized ECM powders previously reported (Supplementary Fig. S1a) [41,51]. FTIR spectra of each lyophilized ECM demonstrated slight differences, presenting different infrared peaks. FTIR spectra of MSC-ECM and HUVEC-ECM powder samples revealed peaks that are unique to each other. Additionally, all four of these unique peaks can also be seen in the IR

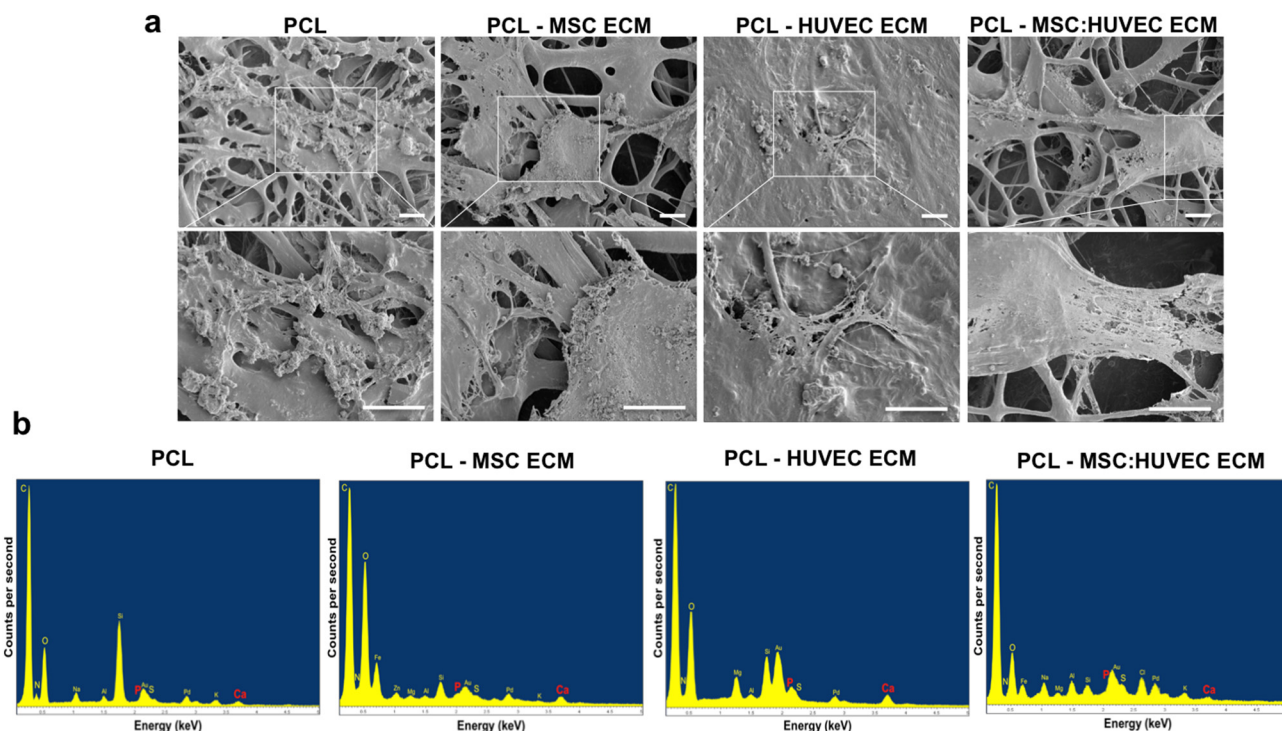


Fig. 5. Morphology and elemental composition analysis of MSCs cultured on cell-derived ECM PCL electrospun fibers and PCL electrospun fibers after 21 days of osteogenic differentiation. SEM images and respective magnification (blank square) (a) and EDS spectrogram (b) for the different cell-derived ECM electrospun scaffolds. Scale bar, 10 μ m.

spectrum of MSC:HUVEC-ECM mixture, suggesting that a combination of cell types in the selected proportion successfully combines components from both types of cell-derived ECM that are known to produce a functional bone matrix. IR peaks correspondent to carbon-hydrogen alkyl bond stretching are also present in all the IR spectra collected (ν -C-H-, 2940–2860 cm^{-1}) (Supplementary Fig. S1b).

In this work, we used electrospinning to fabricate cell-derived ECM electrospun mesh scaffolds with high porosity and interconnectivity, mimicking the architecture and composition of the native bone ECM.

SEM images of cell-derived ECM PCL electrospun fibers clearly revealed the presence of micro/nano-scale cell-derived ECM fragments attached to the fiber surface. The presence of ECM fragments on the fibers was further assessed using Picro-sirius red staining, which stains for the presence of collagens. Results confirmed the presence of collagens in the electrospun scaffolds with incorporated ECM (Supplementary Fig. S3). While immunohistochemistry of specific collagens or other ECM biomolecules should be performed to identify and distinguish more specifically the ECM produced from different cells, such analysis was

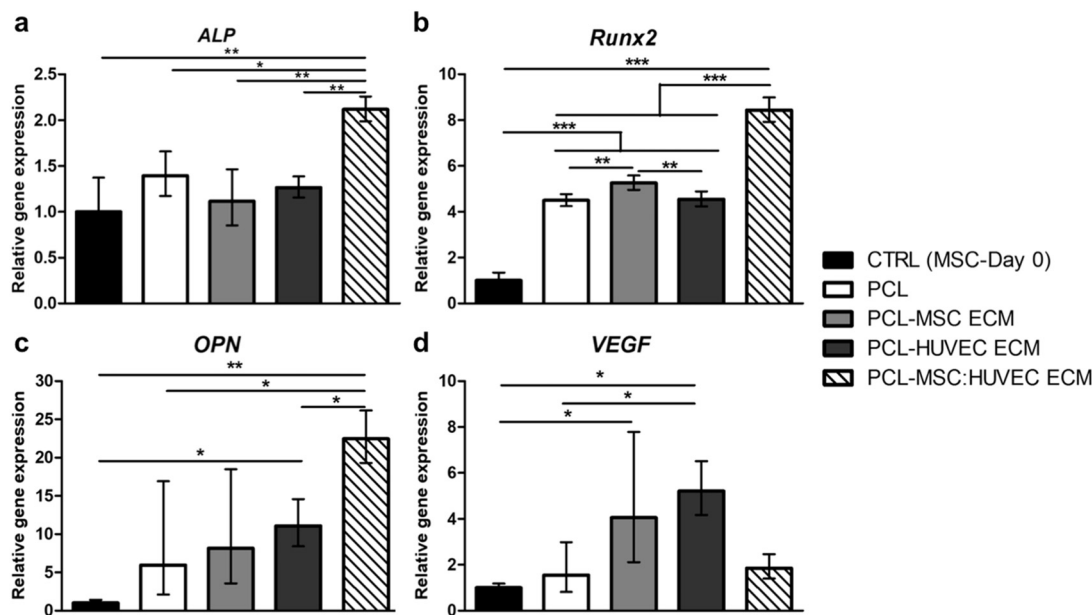


Fig. 6. Effects of cell-derived ECM electrospun scaffolds on ALP (a), Runx2 (b), OPN (c) and VEGF (d) gene expression by MSCs. Results are normalized to the endogenous control GAPDH and presented as fold change expression relative to MSC at day 0. Values are expressed as mean \pm SD (N = 3); * p < 0.05, ** p < 0.01, *** p < 0.001.

beyond the scope of this study, in which the main aim was to evaluate the bioactivity and cellular responses of the ECM-PCL electrospun scaffolds.

Mechanical tensile testing of cell-derived ECM scaffolds demonstrated that the incorporation of the ECM into the PCL scaffolds did not cause the occurrence of critical changes in PCL mechanical properties (Fig. 2). Such properties are reported as promising for bone regeneration applications [22,29], since the scaffold mechanical features mimic native bone ECM and can promote some MSC cellular activities, such as proliferation and mineralization [52,53]. In particular, the mechanical properties of the ECM-PCL electrospun scaffolds including the stiffness are in the range of the values reported for demineralized human cancellous bone by our group [54]. Others have reported that values in this range promote bone repair and regeneration [52] and here we suggest that the mechanisms for such repair and regeneration involve osteogenic differentiation of MSCs as verified by increased ALP activity and osteogenic gene expression levels.

MSCs are a common material to obtain cell-derived ECM due to their ability to deposit ECM that can mimic different tissues depending on culture conditions, including bone, cartilage and adipose tissue. Moreover, MSC-derived ECM has been shown to rejuvenate aged mouse stem cells and enhance their lineage differentiation ability. Decellularized ECM from human MSC cultures have been shown to promote MSCs proliferation [13] and can act as a substrate for chondrocyte proliferation and maintenance of chondrocytic phenotype [55,56]. In addition, HUVEC-derived ECM was used with success to enhance the biocompatibility of pure titanium surfaces [57] whereas Kang and colleagues have fabricated a β -TCP scaffold containing HUVEC-ECM and demonstrated the improved osteogenic capacity of such scaffolds [14]. Co-culture of HUVECs and MSCs have been shown to enhance osteogenic differentiation of MSCs, due to the BMPs secreted by endothelial cells [15]. Therefore, it is expected that ECM produced by MSC:HUVEC co-culture will enhance proliferation and osteogenic differentiation of MSCs, mimicking more accurately the *in vivo* bone niche.

In this study a significant enhancement in proliferation of MSCs seeded on cell-derived scaffolds was observed after 7 days of culture and was maintained after 21 days (Fig. 3a). All the cell-derived ECM microfibrillar scaffolds presented a statistically significant higher cell number when compared to PCL scaffolds alone at days 7, 14 and 21. However, no dramatic differences between the cell-derived scaffolds (MSC-ECM, HUVEC-ECM and MSC:HUVEC-ECM) were observed. We hypothesized that ECM present in these scaffolds may have triggered a faster proliferation due to the signaling molecules and growth factors that were embedded in the ECM. In fact, our results are in accordance with previous findings that showed that the presence of ECM in synthetic scaffolds increased proliferation of MSCs and induced their osteogenic differentiation [14,37,39,45].

Regarding osteogenic differentiation, all the PCL electrospun scaffolds (with and without ECM) promoted osteogenic differentiation of MSCs, as confirmed by the Alizarin Red, ALP/Von Kossa and Xylenol orange staining after 21 days of differentiation. In fact, FDA-approved PCL has been used as electrospun fibers or in other scaffold configurations in bone tissue engineering applications for many years, mainly due to its biochemical/mechanical properties and biocompatibility. Recently, Xue and colleagues [58] showed that PCL electrospun nanofibers were able to enhance osteogenic differentiation potential of MSCs derived from different tissues. Here we found a significant increase of calcium deposition for MSCs cultured on PCL-HUVEC ECM scaffolds, after 21 days of differentiation compared to the other cell-derived ECM scaffolds (Fig. 4b). SEM images also suggest the formation of mineralized nodules after 21 days of osteogenic differentiation (Fig. 5a). This observation is in accordance with work of Fu and colleagues [40], in which they observed the formation of mineralized nodules after 14 days of osteogenic differentiation of mouse bone marrow MSCs in PLLA electrospun scaffolds decorated with ECM generated by mouse

osteoblastic (MC3T3-E1) cells. Moreover, elemental analysis indicated the presence of calcium and phosphorous after 21 days of culture in the electrospun scaffolds, suggesting a successful differentiation of MSCs into osteoblasts (Fig. 5b).

MSCs cultured on PCL-MSC:HUVEC ECM scaffolds presented a significantly higher ALP activity after 14 days of differentiation, compared to PCL scaffolds (Fig. 4a). After 21 days, the ALP activity of MSCs cultured on all electrospun scaffolds decreased, presenting similar results to the ones verified for PCL alone. In fact, during osteogenic differentiation of MSCs, transcription and protein expression of ALP is enhanced as an early marker of osteogenesis [59]. After this peak of ALP activity, its level starts to decline, as we observed for all cell-derived PCL electrospun scaffolds.

Real time quantitative PCR analysis was performed to evaluate the expression of osteogenic marker genes and angiogenic marker *VEGF* in the different scaffolds studied. We decided to evaluate both osteogenic and angiogenic markers together due to the known major role of angiogenesis and vascularization in successful bone regeneration [60,61]. Our gene expression results (Fig. 6) suggest an improved osteogenic potential of PCL-MSC:HUVEC ECM scaffolds compared to the other scaffold conditions. Such statement is supported by the significantly higher expression of *ALP* and *Runx2* markers when MSCs are cultured on PCL-MSC:HUVEC-ECM relative to all the other scaffolds studied. Also, *OPN* upregulation after 21 days of differentiation in PCL-MSC:HUVEC ECM suggests a more mature bone tissue-engineered construct obtained by this condition when compared to the other cell-derived electrospun scaffolds. In fact, our results are in accordance with previously reported literature in which increased expression of osteogenic markers *ALP*, *Runx2* and *OPN* were seen when MSCs were cultured either in MSC-ECM 3D printed PCL/PLGA/ β -TCP composite scaffolds [62] or HUVEC-ECM β -TCP scaffolds [14]. Interestingly, regarding *VEGF* expression, both MSC-ECM and HUVEC-ECM electrospun scaffolds showed upregulation, while PCL-MSC:HUVEC ECM scaffold presented expression levels similar to PCL. However, only cells cultured on PCL-HUVEC-ECM electrospun fibers demonstrated a statistically significant increase in *VEGF* expression levels relative to PCL electrospun scaffolds.

Overall, the results of the current study demonstrated that co-culture MSC:HUVEC-derived ECM PCL electrospun scaffolds promote MSCs proliferation and their osteogenic differentiation *in vitro* by better mimicking the *in vivo* ECM composition and structure. However, further studies such as the optimization of ECM amounts loaded in the scaffold and testing of other MSC/endothelial cell sources to generate ECM might be required to obtain constructs with ideal osteogenic performance. *In vivo* testing of such scaffolds should also be considered.

5. Conclusions

In summary, we have successfully fabricated and characterized cell-derived ECM PCL electrospun scaffolds with improved bioactivity while maintaining the mechanical and physical properties provided by the synthetic material. Our results showed that all cell-derived ECM electrospun scaffolds presented improved MSCs proliferation when compared to synthetic scaffold alone. Moreover, a better osteogenic performance was achieved when the electrospun scaffolds were composed by ECM generated from a co-culture of MSC:HUVEC as demonstrated by a significant enhancement in osteogenic markers gene expression levels, which probably suggests that this condition provides a better mimicry of the *in vivo* bone ECM composition and structure. This work therefore presents, for the first time, the combination of ECM derived from a co-culture of MSCs and endothelial cells with electrospun fibers as a promising strategy to enhance MSCs osteogenic differentiation envisaging a broad range of bone repair applications. Future studies on ECM-containing electrospun scaffolds will also be needed to assess the impact of the surface roughness and the optimal amount and distribution of ECM on MSCs proliferation.

Notes

D.V. has an equity interest in Orthograft L.L.C. All the other authors declare no competing financial interest.

Acknowledgements

This study was supported by funds from the Center of Biotechnology and Interdisciplinary Studies, Rensselaer Polytechnic Institute and the FCT (individual fellowship SFRH/BD/52478/2014 awarded to Marta S. Carvalho and individual fellowship SFRH/BD/105771/2014 awarded to João C. Silva). Funding received by iBB-Institute for Bioengineering and Biosciences from FCT (UID/BIO/04565/2013), from Programa Operacional Regional de Lisboa 2020 (Project N. 007317) is also acknowledged. This work made use of a Leica STED TCS SP8 3x instrument that was acquired through support from the National Science Foundation (Grant# NSF-MRI-1725984), with additional support from New York Capital Region Research Alliance (NYCAP) and the National Institutes of Health (Grant # DK111958).

Author's contributions

M.S.C. and J.C.S. contributed equally to this work. M.S.C., J.C.S, R.J.L. and D.V. conceived and designed the study. M.S.C., J.C.S and R. N. U. carried out the experimental work. M.S.C. and J.C.S. wrote the manuscript. All authors participated in the data analysis, reviewing and editing of the final manuscript.

Appendix A. Supplementary data

Additional experimental results described in the manuscript are included in supplementary information, namely: SEM and FTIR analysis of the different extracellular matrices generated; immunocytochemistry analysis of the different types of cell-derived ECM; Picro-sirius red staining, FTIR analysis and DSC thermograms of all cell-derived ECM-PCL electrospun scaffolds; SEM morphological analysis of MSCs cultured under osteogenic differentiation conditions in the different cell-derived ECM electrospun scaffolds at different culture time points; and a table summarizing the mechanical properties of the different cell-derived ECM electrospun scaffolds fabricated. Supplementary data to this article can be found online at doi:<https://doi.org/10.1016/j.msec.2019.01.127>.

References

- [1] S.F. Badyal, D.O. Freytes, T.W. Gilbert, Extracellular matrix as a biological scaffold material: structure and function, *Acta Biomater.* 5 (2009) 1–13.
- [2] H. Kleinman, L. Luckenbill-Edds, F. Cannon, G. Sephel, Use of extracellular matrix components for cell culture, *Anal. Biochem.* 166 (1987) 1–13.
- [3] A.S. Mistry, A.G. Mikos, Tissue engineering strategies for bone regeneration, *Regenerative Medicine II*, Springer, 2005, pp. 1–22.
- [4] A. Khademhosseini, J.P. Vacanti, R. Langer, *Progress in tissue engineering*, *Sci. Am.* 300 (2009) 64–71.
- [5] A.K. Kundu, A.J. Putnam, Vitronectin and collagen I differentially regulate osteogenesis in mesenchymal stem cells, *Biochem. Biophys. Res. Commun.* 347 (2006) 347–357.
- [6] Y. Ku, C.P. Chung, J.H. Jang, The effect of the surface modification of titanium using a recombinant fragment of fibronectin and vitronectin on cell behavior, *Biomaterials* 26 (2005) 5153–5157.
- [7] S. Bhowmick, S. Rother, H. Zimmermann, P.S. Lee, S. Moeller, M. Schnabelrauch, V. Koul, R. Jordan, V. Hintze, D. Scharnweber, Biomimetic electrospun scaffolds from main extracellular matrix components for skin tissue engineering application—the role of chondroitin sulfate and sulfated hyaluronan, *Mater. Sci. Eng. C* 79 (2017) 15–22.
- [8] B. Beiki, B. Zeynali, E. Seyedjafari, Fabrication of a three dimensional spongy scaffold using human Wharton's jelly derived extracellular matrix for wound healing, *Mater. Sci. Eng. C* 78 (2017) 627–638.
- [9] V. Ryzhuk, X.X. Zeng, X. Wang, V. Melnychuk, L. Lankford, D. Farmer, A. Wang, Human amnion extracellular matrix derived bioactive hydrogel for cell delivery and tissue engineering, *Mater. Sci. Eng. C* 85 (2018) 191–202.
- [10] P.E. Bourguine, C. Scotti, S. Pigeot, L.A. Tchang, A. Todorov, I. Martin, Osteoinductivity of engineered cartilaginous templates devitalized by inducible apoptosis, *PNAS* 111 (2014) 17426–17431.
- [11] R.O. Hynes, The extracellular matrix: not just pretty fibrils, *Science* 326 (2009) 1216–1219.
- [12] L.E. Fitzpatrick, T.C. McDevitt, Cell-derived matrices for tissue engineering and regenerative medicine applications, *Biomater. Sci.* 3 (2015) 12–24.
- [13] Y. Lai, Y. Sun, C.M. Skinner, E.L. Son, Z. Lu, R.S. Tuan, R.L. Jilka, J. Ling, X.D. Chen, Reconstitution of marrow-derived extracellular matrix ex vivo: a robust culture system for expanding large-scale highly functional human mesenchymal stem cells, *Stem Cells Dev.* 19 (2010) 1095–1107.
- [14] Y. Kang, S. Kim, J. Bishop, A. Khademhosseini, Y. Yang, The osteogenic differentiation of human bone marrow MSCs on huvec-derived ECM and B-TCP scaffold, *Biomaterials* 33 (2012) 6998–7007.
- [15] X. Zhao, L. Liu, F.K. Wang, D.P. Zhao, X.M. Dai, X.S. Han, Coculture of vascular endothelial cells and adipose-derived stem cells as a source for bone engineering, *Ann. Plast. Surg.* 69 (2012) 91–98.
- [16] H.H. Luu, W.X. Song, X. Luo, D. Manning, J. Luo, Z.L. Deng, K.A. Sharff, A.G. Montag, R.C. Haydon, T.C. He, Distinct roles of bone morphogenetic proteins in osteogenic differentiation of mesenchymal stem cells, *J. Orthop. Res.* 25 (2007) 665–677.
- [17] J. Ma, J.J.P. van den Beucken, F. Yang, S.K. Both, F.-Z. Chui, J. Pan, J.A. Jansen, Coculture of osteoblasts and endothelial cells: optimization of culture media and cell ratio, *Tissue Eng. Part C* 17 (2010) 349–357.
- [18] Y. Hong, A. Huber, K. Takanari, N.J. Amoroso, R. Hashizume, S.F. Badyal, W.R. Wagner, Mechanical properties and in vivo behavior of a biodegradable synthetic polymer microfiber–extracellular matrix hydrogel biohybrid scaffold, *Biomaterials* 32 (2011) 3387–3394.
- [19] L.G. Bracaglia, J.P. Fisher, Extracellular matrix-based biohybrid materials for engineering compliant, matrix-dense tissues, *Adv. Healthc. Mater.* 4 (2015) 2475–2487.
- [20] W.J. Li, C.T. Laurencin, E.J. Caterson, R.S. Tuan, F.K. Ko, Electrospun nanofibrous structure: a novel scaffold for tissue engineering, *J. Biomed. Mater. Res.* 60 (2002) 613–621.
- [21] T.J. Sill, H.A. von Recum, Electrospinning: applications in drug delivery and tissue engineering, *Biomaterials* 29 (2008) 1989–2006.
- [22] H. Yoshimoto, Y. Shin, H. Terai, J. Vacanti, A biodegradable nanofiber scaffold by electrospinning and its potential for bone tissue engineering, *Biomaterials* 24 (2003) 2077–2082.
- [23] N. Bhardwaj, S.C. Kundu, Electrospinning: a fascinating fiber fabrication technique, *Biotechnol. Adv.* 28 (2010) 325–347.
- [24] N. Reznikov, R. Shahar, S. Weiner, Bone hierarchical structure in three dimensions, *Acta Biomater.* 10 (2014) 3815–3826.
- [25] A. Cipitria, A. Skelton, T. Dargaville, P. Dalton, D. Hutmacher, Design, fabrication and characterization of PCL electrospun scaffolds—a review, *J. Mater. Chem.* 21 (2011) 9419–9453.
- [26] I. Engelberg, J. Kohn, Physico-mechanical properties of degradable polymers used in medical applications: a comparative study, *Biomaterials* 12 (1991) 292–304.
- [27] J.C. Middleton, A.J. Tipton, Synthetic biodegradable polymers as orthopedic devices, *Biomaterials* 21 (2000) 2335–2346.
- [28] L.S. Nair, C.T. Laurencin, Biodegradable polymers as biomaterials, *Prog. Polym. Sci.* 32 (2007) 762–798.
- [29] M.A. Woodruff, C. Lange, J. Reichert, A. Berner, F. Chen, P. Fratzl, J.T. Schantz, D.W. Hutmacher, Bone tissue engineering: from bench to bedside, *Mater. Today* 15 (2012) 430–435.
- [30] X. Li, J. Xie, X. Yuan, Y. Xia, Coating electrospun poly (ε-caprolactone) fibers with gelatin and calcium phosphate and their use as biomimetic scaffolds for bone tissue engineering, *Langmuir* 24 (2008) 14145–14150.
- [31] W. Mattanavee, O. Suwantong, S. Puthong, T. Bunaprasert, V.P. Hoven, P. Supaphol, Immobilization of biomolecules on the surface of electrospun polycaprolactone fibrous scaffolds for tissue engineering, *ACS Appl. Mater. Interfaces* 1 (2009) 1076–1085.
- [32] R.K. Singh, G.Z. Jin, C. Mahapatra, K.D. Patel, W. Chrzanowski, H.W. Kim, Mesoporous silica-layered biopolymer hybrid nanofibrous scaffold: a novel nanobiomatrix platform for therapeutics delivery and bone regeneration, *ACS Appl. Mater. Interfaces* 7 (2015) 8088–8098.
- [33] S.E. Kim, Y.P. Yun, Y.K. Han, D.W. Lee, J.Y. Ohe, B.S. Lee, H.R. Song, K. Park, B.J. Choi, Osteogenesis induction of periodontal ligament cells onto bone morphogenic protein-2 immobilized PCL fibers, *Carbohydr. Polym.* 99 (2014) 700–709.
- [34] Q. Yao, J.G. Cosme, T. Xu, J.M. Miszuk, P.H. Picciani, H. Fong, H. Sun, Three dimensional electrospun PCL/PLA blend nanofibrous scaffolds with significantly improved stem cells osteogenic differentiation and cranial bone formation, *Biomaterials* 115 (2017) 115–127.
- [35] R.A. Thibault, L. Scott Baggett, A.G. Mikos, F.K. Kasper, Osteogenic differentiation of mesenchymal stem cells on pregenerated extracellular matrix scaffolds in the absence of osteogenic cell culture supplements, *Tissue Eng. Part A* 16 (2009) 431–440.
- [36] N. Datta, H.L. Holtorf, V.I. Sikavitsas, J.A. Jansen, A.G. Mikos, Effect of bone extracellular matrix synthesized in vitro on the osteoblastic differentiation of marrow stromal cells, *Biomaterials* 26 (2005) 971–977.
- [37] G. Tour, M. Wendel, I. Tcacencu, Cell-derived matrix enhances osteogenic properties of hydroxyapatite, *Tissue Eng. Part A* 17 (2010) 127–137.
- [38] R. Shtrichman, N. Zeevi-Levin, R. Zaid, E. Barak, B. Fishman, A. Ziskind, R. Shulman, A. Novak, R. Avrahami, E. Livne, The generation of hybrid electrospun nanofiber layer with extracellular matrix derived from human pluripotent stem cells, for regenerative medicine applications, *Tissue Eng. Part A* 20 (2014) 2756–2767.
- [39] H. Jeon, J. Lee, H. Lee, G.H. Kim, Nanostructured surface of electrospun PCL/DEC

- fibres treated with oxygen plasma for tissue engineering, *RSC Adv.* 6 (2016) 32887–32896.
- [40] Y. Fu, L. Liu, R. Cheng, W. Cui, ECM decorated electrospun nanofiber for improving bone tissue regeneration, *Polymers* 10 (2018) 272.
- [41] S. Thakkar, C.A. Ghebes, M. Ahmed, C. Kelder, C.A. Van Blitterswijk, D. Saris, H.A. Fernandes, L. Moroni, Mesenchymal stromal cell-derived extracellular matrix influences gene expression of chondrocytes, *Biofabrication* 5 (2013) 025003.
- [42] B.M. Young, K. Shankar, B.P. Allen, R.A. Pouliot, M.B. Schneck, N.S. Mikhail, R.L. Heise, Electrospun decellularized lung matrix scaffold for airway smooth muscle culture, *ACS Biomater. Sci. Eng.* 3 (2017) 3480–3492.
- [43] S. Gao, M. Chen, P. Wang, Y. Li, Z. Yuan, W. Guo, Z. Zhang, X. Zhang, X. Jing, X. Li, An electrospun fiber reinforced scaffold promotes total meniscus regeneration in rabbit meniscectomy model, *Acta Biomater.* 73 (2018) 127–140.
- [44] S. Baiguera, C. Del Gaudio, E. Lucatelli, E. Kuevda, M. Boieri, B. Mazzanti, A. Bianco, P. Macchiarelli, Electrospun gelatin scaffolds incorporating rat decellularized brain extracellular matrix for neural tissue engineering, *Biomaterials* 35 (2014) 1205–1214.
- [45] M. Gibson, V. Beachley, J. Coburn, P.A. Bandinelli, H.Q. Mao, J. Elisseeff, Tissue extracellular matrix nanoparticle presentation in electrospun nanofibers, *Biomed. Res. Int.* 2014 (2014) 469120.
- [46] T. Gong, B.C. Heng, J. Xu, S. Zhu, C. Yuan, E.C.M. Lo, C. Zhang, Decellularized extracellular matrix of human umbilical vein endothelial cells promotes endothelial differentiation of stem cells from exfoliated deciduous teeth, *J. Biomed. Mater. Res. A* 105 (2017) 1083–1093.
- [47] W.S. Sheridan, G.P. Duffy, B.P. Murphy, Optimum parameters for freeze-drying decellularized arterial scaffolds, *Tissue Eng. Part C Methods* 19 (2013) 981–990.
- [48] A. Aguirre, J. Planell, E. Engel, Dynamics of bone marrow-derived endothelial progenitor cell/mesenchymal stem cell interaction in co-culture and its implications in angiogenesis, *Biochem. Biophys. Res. Commun.* 400 (2010) 284–291.
- [49] S.M. Nassiri, R. Rahbarghazi, Interactions of mesenchymal stem cells with endothelial cells, *Stem Cells Dev.* 23 (2013) 319–332.
- [50] J.K. Mouw, G. Ou, V.M. Weaver, Extracellular matrix assembly: a multiscale deconstruction, *Nat. Rev. Mol. Cell Biol.* 15 (2014) 771.
- [51] C.H. Chang, C.C. Chen, C.H. Liao, F.H. Lin, Y.M. Hsu, H.W. Fang, Human acellular cartilage matrix powders as a biological scaffold for cartilage tissue engineering with synovium-derived mesenchymal stem cells, *J. Biomed. Mater. Res. A* 102 (2014) 2248–2257.
- [52] Q. Hu, M. Liu, G. Chen, Z. Xu, Y. Lv, Demineralized bone scaffolds with tunable matrix stiffness for efficient bone integration, *ACS Appl. Mater. Interfaces* 10 (2018) 27669–27680.
- [53] G. Chen, C. Dong, L. Yang, Y. Lv, 3D scaffolds with different stiffness but the same microstructure for bone tissue engineering, *ACS Appl. Mater. Interfaces* 7 (2015) 15790–15802.
- [54] S. Tang, U. Zeenath, D. Vashishth, Effects of non-enzymatic glycation on cancellous bone fragility, *Bone* 40 (2007) 1144–1151.
- [55] Y. Yang, H. Lin, H. Shen, B. Wang, G. Lei, R.S. Tuan, Mesenchymal stem cell-derived extracellular matrix enhances chondrogenic phenotype of and cartilage formation by encapsulated chondrocytes in vitro and in vivo, *Acta Biomater.* 60 (2018) 71–82.
- [56] H. Lu, T. Hoshiba, N. Kawazoe, I. Koda, M. Song, G. Chen, Cultured cell-derived extracellular matrix scaffolds for tissue engineering, *Biomaterials* 32 (2011) 9658–9666.
- [57] X. Xue, J. Wang, Y. Zhu, Q. Tu, N. Huang, Biocompatibility of pure titanium modified by human endothelial cell-derived extracellular matrix, *Appl. Surf. Sci.* 256 (2010) 3866–3873.
- [58] R. Xue, Y. Qian, L. Li, G. Yao, L. Yang, Y. Sun, Polycaprolactone nanofiber scaffold enhances the osteogenic differentiation potency of various human tissue-derived mesenchymal stem cells, *Stem Cell Res Ther* 8 (2017) 148.
- [59] J.E. Aubin, Regulation of osteoblast formation and function, *Rev. Endocr. Metab. Disord.* 2 (2001) 81–94.
- [60] S. Stegen, N. van Gestel, G. Carmeliet, Bringing new life to damaged bone: the importance of angiogenesis in bone repair and regeneration, *Bone* 70 (2015) 19–27.
- [61] A.S. Curry, N.W. Pensa, A.M. Barlow, S.L. Bellis, Taking cues from the extracellular matrix to design bone-mimetic regenerative scaffolds, *Matrix Biol.* 52 (2016) 397–412.
- [62] F. Pati, T.-H. Song, G. Rijal, J. Jang, S.W. Kim, D.-W. Cho, Ornamenting 3D printed scaffolds with cell-laid extracellular matrix for bone tissue regeneration, *Biomaterials* 37 (2015) 230–241.